Eur. Phys. J. D **26**, 91–98 (2003)
DOI: 10.1140/epjd/e2003-00072-2

THE EUROPEAN PHYSICAL JOURNAL D

Applications of high-order harmonics

A. L'Huillier[a], D. Descamps[b], A. Johansson, J. Norin, J. Mauritsson, and C.-G. Wahlström

Department of Physics, Lund Institute of Technology, P.O. Box 118, 221 00 Lund, Sweden

Received 11 December 2002
Published online 24 April 2003 –

Abstract. We review applications of high-order harmonic generation in different fields of physics, from spectroscopic studies of atoms and molecules, to interferometry and plasma diagnostics and nonlinear optics.

PACS. 32.80.Fb Photoionization of atoms and ions – 42.65.Ky Frequency conversion; harmonic generation, including higher-order harmonic generation

1 Historical background

When an intense laser pulse is focused into a gas of atoms, high-order harmonics of the fundamental radiation can be emitted. The first experimental observations of these phenomena, which showed the characteristic harmonic plateau, were done in Chicago [1] and in Saclay [2] at the end of the 80's. Most of the early work concentrated on the extension of the plateau, *i.e.* the generation of harmonics of higher frequency and shorter wavelength going progressively from ∼20 nm at the end of the 80's to ∼7 nm in the mid 90's. Today, harmonic spectra produced with short and intense laser pulses extend to the water window (below the carbon K-edge at 4.4 nm) [3,4]. A breakthrough in the theoretical understanding of high-order harmonic generation processes in low frequency laser fields was initiated by Krause and coworkers [5] who showed that the cut-off position in the harmonic spectrum follows the universal law $I_\mathrm{p} + 3U_\mathrm{p}$, where I_p is the ionization potential and U_p is the ponderomotive potential, *i.e.* the mean kinetic energy acquired by an electron oscillating in the laser field. An explanation of this universal fact in the framework of a "simple man's theory" was found shortly afterwards [6,7]. A fully quantum mechanical theory, that is based on a strong field approximation (SFA) and that recovers the simple man's theory, was then formulated [8,9]. Progress in experimental techniques and theoretical understanding stimulated numerous studies of optimization and control of harmonic generation. These studies involved among others, optimization of the laser parameters, generation by multicolored fields, optimization of the generating medium, and characterization and optimization of the spatial and temporal properties (see references in [10–12]).

Very rapidly, it was realized that the radiation presented unique characteristics, of interest for applications. The first application of the harmonic radiation was done as early as in 1993 and consisted in studying the time evolution of surface states using a pump/probe technique [13]. The properties of the harmonic emission (ultrashort pulse duration, high brightness, good coherence) make it a unique source of XUV radiation, which is now used in a growing number of applications ranging from atomic [14–17] and molecular [18–20] spectroscopy to solid-state [13,21,22] and plasma [23–25] physics. The harmonic radiation is intense enough to induce nonlinear optical processes in the XUV range, as recently demonstrated by [26–28]. It can also be used to generate extremely short (attosecond) light pulses [29,30].

In the present paper, we review some of these applications, and in particular those performed in Lund. In Section 2, we present lifetime (and photoionization cross-section) measurements performed in He, CO, N_2, C_2H_2 and C_2D_2 in the picosecond and femtosecond regimes. The advantage of using harmonics in XUV interferometry measurements is pointed out in Section 3. In Section 4, we review the present status regarding multiphoton experiments using harmonics. We conclude in Section 5.

2 Applications in atomic and molecular spectroscopy

In all our experiments using harmonics in atomic and molecular spectroscopy, we have used a pump/probe setup, with a short harmonic pulse for the excitation of an electronic state and a short laser pulse for the analysis. The different cases studied in Lund from 1995 until

[a] e-mail: anne.lhuillier@fysik.lth.se
[b] *Present address*: CEA/DRECAM/SPAM, CEN Saclay, 91105 Gif-sur-Yvette, France.

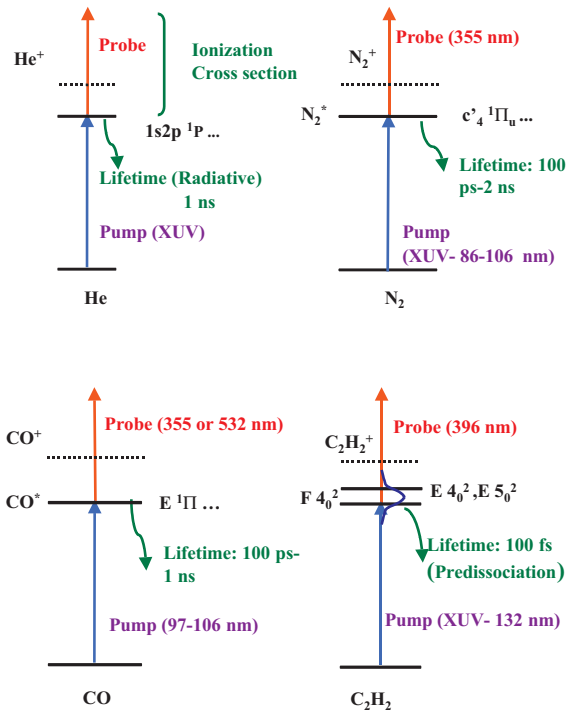

Fig. 1. Energy level diagram of He, CO, N_2, C_2H_2 indicating some of the atomic or molecular states studied and the two-photon ionization schemes.

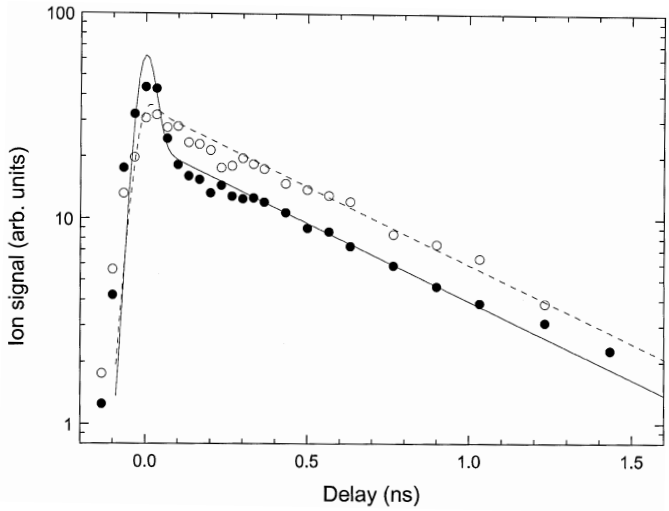

Fig. 2. He^+ ion signal as a function of the temporal delay between the pump and the probe pulse. The open circles and dashed line show the exponentional decay curve recorded upon excitation of the He $1s2p$ ^{1}P state; the filled circles and solid line show an enhancement of the zero-time delay signal due to resonant absorption of the pump and AC Stark broadening of the transition.

now are schematized in Figure 1. For He, CO and N_2, we use a distributed feedback dye laser (DFDL), amplified in a titanium-sapphire crystal, delivering 70 ps 35 mJ pulses tunable in the infrared [31,32]. For example, the He $1s2p$ ^{1}P state is excited by the 13th harmonic of the fundamental radiation tuned to a 759 nm wavelength, and ionized by visible or ultraviolet radiation. The He $1s3p$ ^{1}P state is excited by the 14th harmonic obtained by first frequency doubling the infrared laser. In general, we let both fundamental and second harmonic radiations interact with the Kr gas jet where the XUV radiation is generated. Using the tunability of our laser system together with the possibility to generate both even and odd harmonics in this way, a quasi-tunability from 40 to 200 nm is achieved.

It is important for these experiments to work with a short laser pulse (compared to the lifetime to be measured) and a narrow bandwidth, in order to optimize the excitation process. We measure spectral widths of the order of 3.5 pm (1.3 meV) for the 13th harmonic, which can be compared to a Doppler width of 0.13 meV for the He $1s2p$ ^{1}P level. The lifetimes of excited states are determined by varying the temporal delay between the pump (XUV) and the probe (UV-visible) pulse and recording the number of ions produced. A typical decay curve of the He $1s2p$ ^{1}P state is displayed in Figure 2 (open circles, dashed line), showing on a logarithmic scale the number of He^+ ions as a function of the delay time.

The photon energy of the probe laser is chosen so that the excited $1snp$ ^{1}P states get ionized in the region close to threshold, thus optimizing the ionization cross-section and preventing the ionization of lower-lying He $1sns$ ^{1}S states, which can be populated by radiative relaxation. For the He $1s2p$ ^{1}P resonance, we use a probe energy of 3.5 eV (355 nm). The decay curves (see dashed line in Fig. 2) show clearly that the logarithm of the signal varies linearly with the delay time, allowing us to determine the lifetime with good accuracy. The measurements yield lifetimes of 0.57 ± 0.03 ns for the $1s2p$ state and 1.76 ± 0.1 ns for the $1s3p$ state, in good agreement with previous data having about the same level of precision (5%). In some conditions, at relatively high pressure, we find that the exponential decay can be perturbed by a significant enhancement of the number of ions at very short time delays (solid line in Fig. 2). This effect is attributed to a "direct" two-photon ionization process, which is enhanced relatively to (time-delayed) pump-probe ionization, owing to a combination of resonant absorption of the XUV light and AC-Stark broadening of the excited level.

Photoionization cross-sections are determined by recording the number of He^+ ions, for fixed photon energies of the pump and the probe beams, as a function of the energy in the probe beam, *i.e.* the number of probe photons [17,31]. A typical experimental result obtained for He $1s2p$ with a probe wavelength of 355 nm is presented in Figure 3 (top).

The ion signal varies first linearly with the probe energy (see dashed line), and then saturates, because the ionization probability in the interaction region is close to one. Knowing the spatial profiles of both the pump and the probe beams, as well as the energy in the probe beam, the absolute value of the ionization cross-section is determined by fitting the experimental data. The experimental results for the determination of the absolute cross-section of the excited He $1s3p$ state, using a parallel orientation between

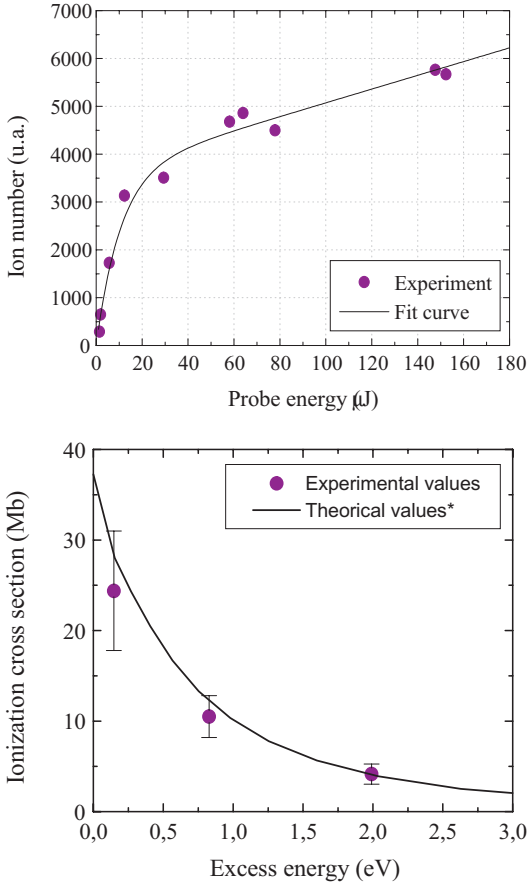

Fig. 3. (top) He^+ ion signal as a function of the energy of the probe pulse. He atoms are prepared in the He $1s2p$ excited state and the probe laser is set to a wavelength of 355 nm. The dashed line indicates the linear, unsaturated regime. The solid line represents a fit to the experimental data; (bottom) photoionization cross-section from the He $1s2p$ excited state as a function of the probe photon energy; experimental cross-sections (solid circles); theoretical data (solid line) [33].

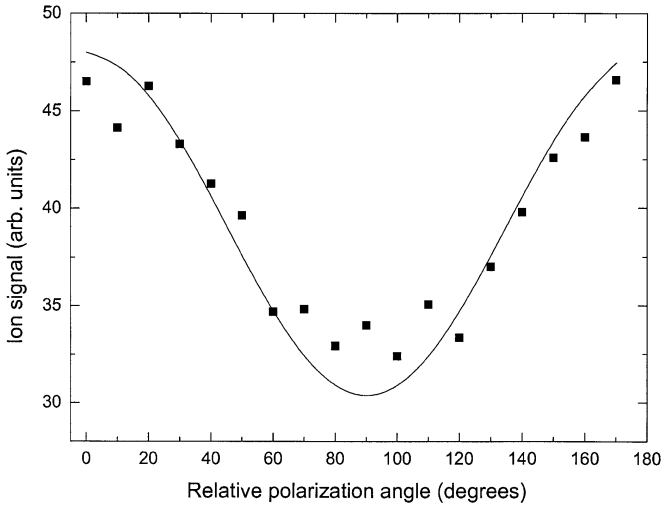

Fig. 4. He^+ ion signal as a function of angle between the polarization vectors of the pump and the probe beams. The theoretically predicted variation of the relative cross-section [33] is indicated by the solid curve.

the polarization vectors of the pump and the probe beam, shown in Figure 3 (bottom) compare well with theoretical data [33,34]. In addition, the well defined linear polarization of the pump and probe pulses allows us to extract the partial ionization cross-sections by changing the relative orientation of their polarization vectors. The variation of the number of He ions as a function of the angle θ_P between the polarization vectors is shown in Figure 4, together with

$$\sigma(\theta_P) = \sigma_s + \sigma_d + 2\left(\sigma_s + \frac{1}{10}\sigma_d\right) P_2(\cos\theta_P),$$

using the theoretical ratio [33] $\sigma_d/\sigma_s = 13/1$. The given example demonstrates the potential of this type of pump-probe experiments to provide detailed information on the photoionization process by simply measuring the total ion signal.

The same experimental technique (and the same laser system) has also been used for lifetime measurements of excited states of CO [15] and N_2 [16]. The wavelength of the radiation needed to excite these states varies between 83 and 106 nm requiring the use of the 8th or the 7th harmonic of the DFDL and the lifetimes are between 100 ps and 2 ns. In N_2, the lifetimes of the electronic states $c_4' \, ^1\Sigma_u^+$, $c_4 \, ^1\Pi_u$, $c_3 \, ^1\Pi_u$, $o_3 \, ^1\Pi_u$, $b \, ^1\Pi_u$, in the vibrational states $v = 0$ or 1, have been determined for several isotopomers. In CO, the electronic states studied have been the $C \, ^1\Sigma^+$, $E \, ^1\Pi$ and $L \, ^1\Pi$. One goal of this research, of interest in astrophysics, is to determine the importance of predissociation, and its dependence on the isotope. Our measurements give the total lifetime of the states, while the radiative lifetime is determined from calculated oscillator strengths.

A similar setup, using pump/probe pulses in the 100 fs range and photoelectron spectroscopy to monitor the decay has been used to study dissociation of Rydberg states in acetylen and deuterated acetylen [18,35]. Electronic states lying in the $4s-3d$ Rydberg supercomplex are excited by the third harmonic (∼132 nm) of the (396 nm) frequency doubled laser radiation and ionized after a variable time delay by a 396 nm laser pulse. The photoelectron spectrum provides an insight on the different initial electronic states populated. However, the high density of initial states prepared by the short XUV pulse sometimes leads to overlaps of the photoelectron spectra. In order to study the dynamics of each initial state in spite of these overlaps, the frequency of the pump laser is sweeped throughout the pulse. The excited states come into resonance at different times. Their dissociation dynamics have different initial times, and can thus be analyzed separately.

The experimental setup for these experiments is shown in Figure 5. The 396 nm-pulse used to generate high-order harmonics and the time-delayed 396 nm-probe pulse are generated through frequency doubling of a titanium sapphire laser in KDP crystals in a modified Michelson interferometer. A negative lens is inserted in one of the beam

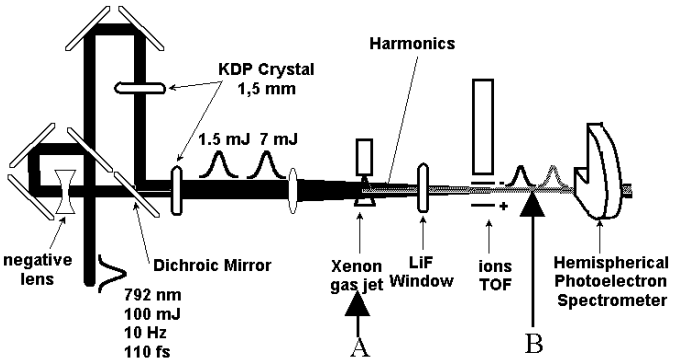

Fig. 5. Experimental setup for the study of predissociative states in acetylen.

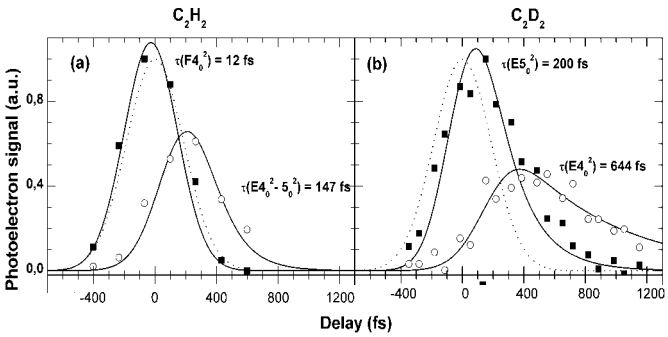

Fig. 7. Photoelectron signal as function of pump-probe delay (a) in C_2H_2 and (b) in C_2D_2. The fits from the multifit procedure [35] are shown in solid line. The dashed line is the fit to the cross-correlation signal.

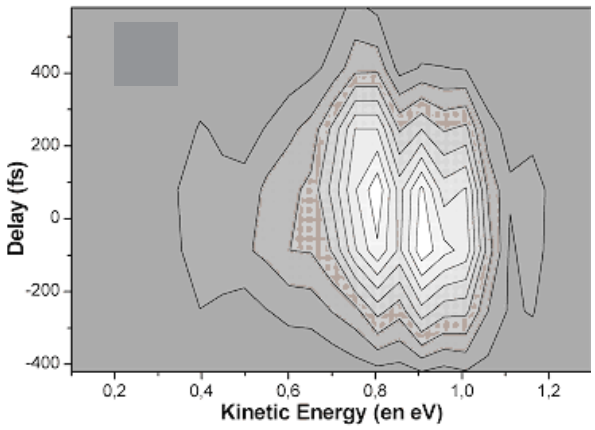

Fig. 6. Number of electrons as a function of electron energy and time delay in C_2H_2. The contour plot shows two main structures in energy with a clear difference in temporal dynamics.

paths to focus the two pulses at different locations. This setup allows us to produce pairs of 396 nm pulses, and to control the delay between them. The first beam is focused under the nozzle of a xenon gas jet (point A) to generate harmonics and the second (probe) beam is focused about 1.3 m after the jet (point B). A lithium-fluoride (LiF) window placed after the gas jet eliminates all harmonics of order higher than the third. Positive ions are collected in a time-of-flight spectrometer. The photoelectron spectrometer is a truncated hemispherical electrostatic analyzer with a 100 meV resolution.

In Figure 6, the number of electrons emitted as a function of energy and time delay in C_2H_2 using a pump wavelength centered at $\lambda = 132.0$ nm is represented as a contour plot. The spectrum appears to have two different features, which follow different temporal developments. The feature on the right side of the figure corresponds to the excitation of the $F4_0^2$ state, which starts first and leads to the highest kinetic energy electrons. The feature on the left side of the figure is related to excitation of the quasi-degenerate state $E4_0^2 - E5_0^2$. In the same way, in C_2D_2, two states are excited at different times during the pump pulse: first the $E4_0^2$ valence state, then the $E5_0^2$ state.

The time dependence of each spectral component is presented in Figure 7, together with a fit to the data. The dashed line presents the results of a cross-correlation measurement, thus indicating our temporal resolution. A multifit procedure using ion and electron signals in both isotopes, as well as the cross-correlation signal allows us to determine the chirps of both pump and probe pulses as well as the lifetimes of the states. The lifetime of the $F4_0^2$ state in C_2H_2 is very short, below our temporal resolution (a few tens of fs). The lifetime of the $E4_0^2 - E5_0^2$ state is 147 fs. In C_2D_2, we get 200 fs for the $E5_0^2$ state and 644 fs for $E4_0^2$. It would be interesting to characterize independently the pump and probe pulses, using for example the technique presented in [36].

This kind of experiments would benefit from the use of an XUV femtosecond probe pulse, with an energy high enough to reach the ionization continuum of the dissociation product. By recording the photoelectron spectra, it should be possible to follow the dissociation dynamics of the molecule in time. A step in that direction has been recently taken by Nugent-Glandorf and coworkers [20]. They have excited bromine molecules with a 400 nm pump pulse and analyzed the dissociation with a high harmonic pulse (the 17th harmonic of a 800 nm laser). We expect to see an increase in this type of applications of high-order harmonics during the next few years.

3 Applications in interferometry and holography

Two spatially separated sources of high harmonic radiation created by the same laser pulse are phase locked and interfere when superposed in the far field [37,38]. This property can be used to perform interferometry in the XUV range without the use of complex XUV beam splitters and to probe thin solid films and dense plasmas.

The experimental setup used in these experiments is shown in Figure 8. The 800 nm femtosecond laser pulse is split into two identical pulses in a Michelson interferometer. In one arm, a mirror is slightly tilted so that focusing

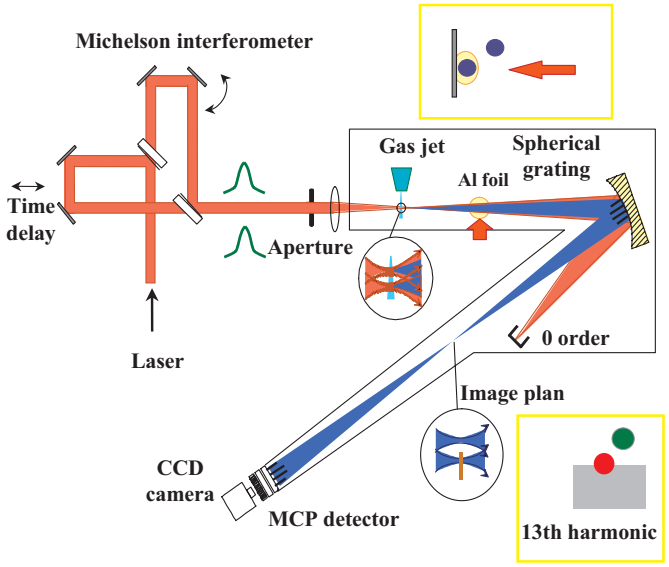

Fig. 8. Principle of the XUV interferometer.

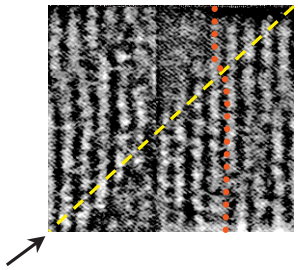

Fig. 9. Interference pattern with the 13th harmonic through an aluminium step filter. The envelope of the spatial distribution of the harmonic beam is removed by using a Fourier transform technique.

of the laser beam results in two spatially separated foci. A normal incidence spherical grating is used to select a given harmonic order and to image with a magnification of one the gas jet plane. From the image plane, the two harmonic beams diverge and overlap in the far field, resulting in an interference pattern, which is observed with microchannel plates coupled to a phosphor screen. The far field fringe pattern can be observed with single shot acquisition and exhibits a good contrast, better than 30% over a large part of the harmonic beam. The two harmonic sources with a diameter $\sim$25 μm, are separated by $\sim$130 μm.

An interferometry image of a free-standing aluminium step filter, obtained with the 11th harmonic is shown in Figure 9. One harmonic beam (probe beam) goes through the center of the filter (containing the step) while the other (reference beam) passes only through the thin layer, uniform enough not to distort the beam (see the inset at the bottom of Fig. 8). The Al filter is placed 15 mm after the image plane. This position is such that the two beams are still spatially separated, but sufficiently far away from the beam waist to ensure that the filter is probed by relatively large beams, and that the image observed on the MCP can

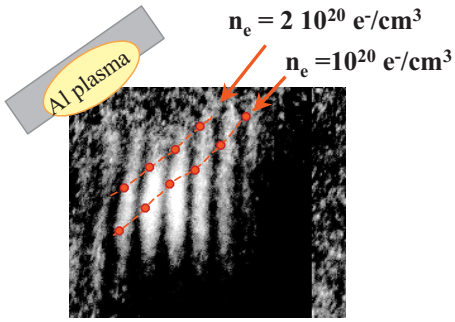

Fig. 10. Single-shot interference pattern obtained with the 11th harmonic. The position of the plasma is shown in the figure, together with isodensity lines (dashed lines).

be considered as a projection of the filter. The top part of the image is the reference fringe pattern while the bottom part includes the phase effect due to the larger thickness of aluminium in the path of one beam. The two parts are clearly separated by a blurred region, which corresponds to the step. A fringe shift of 0.4 is measured between the two fringe patterns, which gives a value of about 70 nm (within a multiple of λ) for the aluminium step size. Similar interference patterns are obtained for the 9th, 11th and 15th harmonics, with a fringe shift varying from 0.7 to 0.3, according to the dispersion of aluminium in this spectral region. This allows us to determine unambiguously the aluminium step size to be 70 nm.

Our technique can also be used to probe laser-produced plasmas. It is well-known that a dense plasma refracts and absorbs visible light. Both absorption and refraction increase with the plasma density as well as with the wavelength of the probe beam. The wavelength of the beam used to probe plasma densities must therefore be short, but not too short since the plasma refractive index approaches unity at very short wavelengths (which makes interferometry measurements difficult). The availability of many odd harmonics allows us, for a given plasma density range, to choose a wavelength for the probe, short enough to avoid refraction and absorption, but long enough to induce a significant dephasing of the beam when propagating through the plasma. The plasma is generated by irradiating a solid target with a 50 mJ, 300 ps, 790 nm-laser pulse, focused on a 50 μm-thick aluminium foil fixed on a flat glass support. In contrast to the filter experiment, we place the target directly after the gas jet plane to reduce as much as possible the influence of the (bright) plasma self emission on the measurements (see the inset at the top of Fig. 8). The optimum probe wavelength to study this particular plasma is found to be that of the 11th harmonic. A single-shot interference pattern is presented in Figure 10, together with the (approximate) position of the Al target. The noise level is higher than without the plasma owing to self-emission and the fringes are tilted. Isodensity lines corresponding to electron densities equal to 1 and 2×10^{20} electrons/cm^3 (from the bottom to the top) are indicated in the figure as dashed lines.

In a recent experiment, Bartels and coworkers have demonstrated that the harmonic radiation could also be

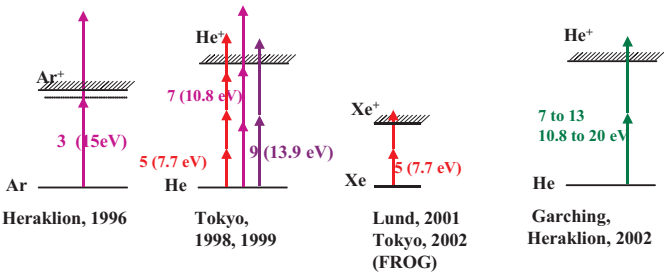

Fig. 11. Summary of the multiphoton processes observed involving high-order harmonics.

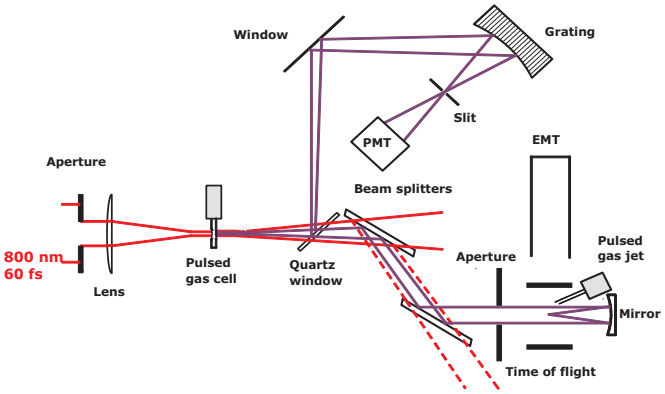

Fig. 12. Experimental setup for the observation of multiphoton processes using the fifth harmonic.

used in holography experiments [39]. The principle of the setup is very simple. An object is placed in the path of the harmonic beam. This leads to diffraction fringe patterns, which can be recorded at some distance from the object. The spatial coherence of the harmonic beam allows them to reconstruct the object (the tip of a near-field scanning optical microscope). The harmonic source by its simplicity and its extremely good spatial coherence properties should become very useful for metrology applications in general.

4 Nonlinear optics using harmonics

The few attempts to observe non-linear processes using high-order harmonics are summarized in Figure 11. Xenakis and coworkers observed resonant (1+1) two-photon ionization in Ar, using the third harmonic (15 eV) of a KrF laser [40]. Watanabe and coworkers report the observation in He of two-photon ionization using the ninth harmonic of a titanium sapphire (Ti:S) laser, four-photon ionization using the fifth harmonic [26,27] and recently, two photon ionization frequency-resolved temporal gating measurement of the fifth harmonic generated in xenon [41]. Recently, we observed non-resonant two-photon ionization in xenon and krypton using the fifth harmonic (7.7 eV) of a Ti:S laser, as well as a quasi-resonant three-photon ionization in argon [28]. Papadogiannis and coworkers observed two-photon ionization of helium, using a combination of the 9th to 13th harmonics [42].

Our experimental setup is shown in Figure 12. The laser is an amplified Ti:S 10 Hz system delivering 60 fs pulses around 800 nm with an energy up to 200 mJ. The beam is apertured down by an 11 mm-diameter diaphragm, so that only about 3 mJ infrared energy is actually sent into the experimental setup. The beam is focused by a 2-m focal length-lens into a 3 mm-long windowless Xe gas cell. A 500 μm thick high-quality UV-grade fused silica plate is used to absorb harmonics of order higher than the fifth. This plate reflects 1% of the beam into an XUV spectrometer, which records the fifth harmonic flux without cutting part of the beam. The fundamental field is eliminated by two beam splitters, antireflection coated at 800 nm, with a reflectivity less than 1% at the fundamental wavelength and about 40% at the fifth harmonic frequency. The harmonic beam is focused by a normal incidence 10-cm focal length spherical mirror, with MgF_2-protected aluminum coating. The gas medium in the interaction region is provided by a pulsed gas jet. The ions produced are detected in a time-of-flight spectrometer.

A major difficulty is to eliminate the influence of other ionization processes, such as multiphoton ionization due to the remaining fundamental laser field, one-photon ionization due to higher-order harmonics, and ionization processes involving mixing of several harmonic or fundamental frequencies. The fundamental field is eliminated essentially by the two beam splitters which decrease the infrared intensity by at least a factor 10^4. The higher-order harmonics are absorbed by the thin fused silica plate, which has a huge absorption coefficient for wavelengths shorter than 160 nm. The group-velocity dispersion in the fused silica plate allows us to separate in time the fundamental, third and fifth harmonic pulses. This ensures that no mixing processes take place in the interaction region. Finally, ionization with third harmonic photons occurs *via* absorption of three photons in Xe, and four photons in Kr and Ar, and therefore requires a higher intensity than for two-photon ionization (or quasi-resonant three-photon ionization). In addition, the ion signal disappears when a (thick) fused silica window, absorbing the fifth harmonic, but not the third, is placed in the beam.

The clearest evidence that the observed signal is due to a two-photon ionization process is shown in Figure 13. The number of ions detected in Xe (a) and in Kr (b) is plotted as a function of the number of fifth harmonic photons. The number of photons is varied by changing the pressure in the gas cell where the harmonics are generated, keeping all other experimental parameters constant. We measure a slope of 2.0 ± 0.2 in Xe and 1.8 ± 0.2 in Kr, over more than two orders of magnitude. The intensity of the fifth harmonic is estimated to be of the order (or below) 4×10^{11} W/cm^2. It should be possible to multiphoton ionize rare gases also with higher-order harmonics, since the number of photons that can be obtained in the 7th, 9th or 11th harmonics, for example, are very close to the number of photons in the fifth harmonic. However, the separation of the different ionization processes that can take place during the interaction is more difficult. One way is to

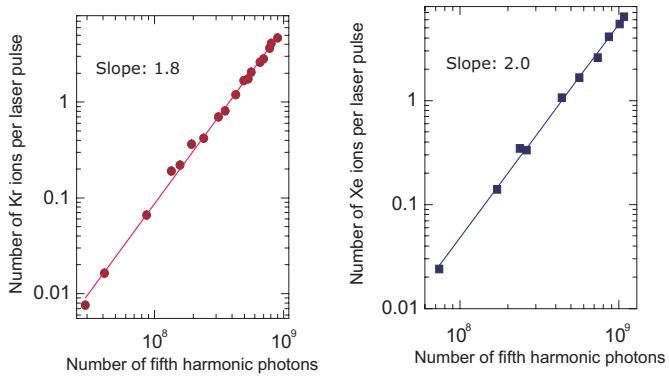

Fig. 13. Number of ions in Xe (a) and Kr (b) as a function of number of fifth harmonic photons.

use an electron spectrometer to identify these processes. These results are important because they open up the field of multiphoton processes and non-linear optics in general to the VUV and XUV regions. Using higher harmonics, it should be possible, for example, to ionize inner-shell electrons by multiphoton processes. In addition, it provides a way to measure ultrashort, femtosecond and even attosecond pulse durations in the VUV and XUV regions by autocorrelation.

5 Conclusion

The field of research "atoms in strong laser fields", though quite fundamental, has led to an interesting new tool for science. The harmonic radiation, with its unique properties of ultrashort pulse duration, high brightness and good spatial and temporal coherence, is being used in a growing number of applications, ranging from atomic and molecular spectroscopy to solid-state and plasma physics. It has also been proposed as an alternative source for nanolithography, in particular for metrological purposes. It opens up two new fields of research: multiphoton processes in the XUV range, demonstrated for the first time three years ago, and attosecond physics, where processes in atoms and molecules can be studied at an unprecedented time scale. Attophysics is just born and there is already an active discussion on the possible applications of attosecond XUV pulses. The first step towards the use of attosecond pulses has been recently taken by Krausz and his collaborators who have been able to "steer" electron wavepackets, generated by attosecond XUV pulses, in the laser light [43] as well as to time resolve an Auger process [44].

We have presented different applications using high-order harmonic radiation as an XUV source. The diversity of these experiments demonstrates the high potential of this new source. The generation of high-order harmonics is experimentally easy to realize. The radiation is relatively intense, and presents interesting properties, often complementary to those of other XUV radiation sources, *e.g.* synchrotrons. In the next few years, we expect the high-order harmonic radiation to become more and more useful in many scientific areas.

This talk was presented at a Special Symposium "Coherent and strong field interactions of laser radiation with matter" in the Honor of Peter Lambropoulos. One of the authors, A.L., wants to thank P.L. for good collaboration and support during many years. Many of the experiments mentioned have been done in collaboration with different European groups. We thank S. Aloise, M. Gisselbrecht and M. Meyer, Orsay; P. Cacciani, Lille; J.P. Sprengers, F. Brandi and W. Ubachs, Amsterdam; S. Zamith, V. Blanchet, B. Girard, Toulouse; J. Andersson, S.L. Sorensen, Lund; I. Hjelte, O. Björneholm, Uppsala; D. Gauyacq, Orsay; J.-F. Hergott, H. Merdji, P. Salières, Saclay; M. Bellini, T.W. Hänsch, Florence. We also thank our former students, postdocs and colleagues C. Lyngå, L. Roos, C. Delfin, R. Zerne, J. Larsson, E. Mevel, S. Buil, V. Lokhnygin and S. Svanberg. We acknowledge the support of the European Community (contracts No. ERBFMGECT-950020, No. ERBFMBICT-983348, No. HPRN-CT-2000-00133), the Swedish Natural Science Research Council and the Göran Gustafsson Foundation for Research in Natural Sciences and Medicine.

References

1. A. McPherson, G. Gibson, H. Jara, U. Johann, T.S. Luk, I. McIntyre, K. Boyer, C.K. Rhodes, J. Opt. Soc. Am. B **4**, 825 (1987)
2. M. Ferray, A. L'Huillier, X.F. Li, L.A. Lompré, G. Mainfray, C. Manus, J. Phys. B **21**, L31 (1988)
3. Z. Chang, A. Rundquist, H. Wang, M.M. Murnane, H.C. Kapteyn, Phys. Rev. Lett. **79**, 2967 (1997)
4. C. Spielmann, N. Burnett, S. Sartania, R. Koppitsch, M. Schnurer, C. Kan, M. Lenzner, P. Wobrauschek, F. Krausz, Science **278**, 661 (1997)
5. J.L. Krause, K.J. Schafer, K.C. Kulander, Phys. Rev. Lett. **68**, 3535 (1992)
6. K.C. Kulander, K.J. Schafer, J.L. Krause, in *Super-Intense Laser-Atom Physics*, edited by B. Piraux, A. L'Huillier, K. Rzążewski, NATO ASI Series B (Plenum Press, New York, 1993), Vol. 316, p. 95
7. P.B. Corkum, Phys. Rev. Lett. **71**, 1994 (1993)
8. A. L'Huillier, M. Lewenstein, P. Salières, Ph. Balcou, M.Yu. Ivanov, J. Larsson, C.-G. Wahlström, Phys. Rev. A **48**, R3433 (1993)
9. M. Lewenstein, Ph. Balcou, M.Yu. Ivanov, A. L'Huillier, P. Corkum, Phys. Rev. A **49**, 2117 (1994)
10. P. Salières, A. L'Huillier, Ph. Antoine, M. Lewenstein, Adv. At. Mol. Opt. Phys. **41**, 83 (1999)
11. P. Salières, M. Lewenstein, Meas. Sci. Tech. **12**, 1818 (2001)
12. T. Brabec, F. Krausz, Rev. Mod. Phys. **72**, 545 (2000)
13. R. Haight, D.R. Peale, Phys. Rev. Lett. **70**, 3979 (1993)
14. J. Larsson, E. Mevel, R. Zerne, A. L'Huillier, C.-G. Wahlström, S. Svanberg, J. Phys. B **28**, L53 (1995)
15. P. Cacciani, W. Ubachs, P.C. Hinnen, C. Lyngå, A. L'Huillier, C.-G. Wahlström, Astrophys. J. **499**, L223 (1998); Eur. Phys. J. D **15**, 47 (2001)
16. W. Ubachs, R. Lang, I. Velchev, W.-Ü.L. Tchang-Brillet, A. Johansson, Z.S. Li, V. Lokhnygin, C.-G. Wahlström, Chem. Phys. **270**, 215 (2001)
17. M. Gisselbrecht, D. Descamps, C. Lyngå, A. L'Huillier, C.-G. Wahlström, M. Meyer, Phys. Rev. Lett. **82**, 4607 (1999)
18. S.L. Sorensen, O. Björneholm, S. Buil, D. Descamps, I. Hjelte, T. Kihlgren, A. L'Huillier, J. Norin, S. Svensson,

S. Sundin, C.-G. Wahlström, G. Öhrwall, J. Chem. Phys. Lett. **112**, 8038 (2000)
19. M. Bauer, C. Lei, K. Read, R. Tobey, J. Gland, M.M. Murnane, H.C. Kapteyn, Phys. Rev. Lett. **87**, 025501 (2001)
20. L. Nugent-Glandorf, M. Scheer, D.A. Samuels, A.M. Mulhisen, E.R. Grant, X. Yang, V.M. Bierbaum, S.R. Leone, Phys. Rev. Lett. **87**, 193002 (2001)
21. F. Quéré, S. Guizard, G. Petite, Ph. Martin, H. Merdji, B. Carré, J.-F. Hergott, Phys. Rev. B **61**, 9883 (2000)
22. T. Sekikawa, T. Ohno, Y. Nabekawa, S. Watanabe, J. Lumin **87**, 827 (2000)
23. W. Theobald, R. Hässner, C. Wülker, R. Sauerbrey, Phys. Rev. Lett. **77**, 298 (1996)
24. P. Salières, L. Le Déroff, T. Auguste, P. Monot, P. d'Oliveira, D. Campo, J.-F. Hergott, H. Merdji, B. Carré, Phys. Rev. Lett. **83**, 5483 (1999)
25. D. Descamps, C. Lyngå, J. Norin, A. L'Huillier, C.-G. Wahlström, J.-F. Hergott, H. Merdji, P. Salières, M. Bellini, T.W. Hänsch, Opt. Lett. **25**, 135 (2000)
26. Y. Kobayashi, T. Sekikawa, Y. Nabekawa, S. Watanabe, Opt. Lett. **23**, 64 (1998)
27. T. Sekikawa, T. Ohna, T. Yamazaki, Y. Nabekawa, S. Watanabe, Phys. Rev. Lett. **83**, 2564 (1999)
28. D. Descamps, L. Roos, C. Delfin, A. L'Huillier, C.-G. Wahlström, Phys. Rev. A **64**, 031401(R) (2001)
29. P.M. Paul, E.S. Toma, P. Breger, G. Mullot, F. Augé, Ph. Balcou, H.G. Muller, P. Agostini, Science **292**, 1689 (2001)
30. M. Hentschel, R. Klenberger, Ch. Spielmann, G.A. Reider, N. Milošević, T. Brabec, P. Corkum, U. Heinzmann, M. Drescher, F. Krausz, Nature **414**, 511 (2001)
31. A. Johansson, M.K. Raarup, Z.S. Li, V. Lokhnygin, D. Descamps, C. Lyngå, E. Mevel, J. Larsson, C.-G. Wahlström, S. Aloise, M. Gisselbrecht, M. Meyer, A. L'Huillier, Eur. Phys. J. D **22**, 3 (2003)
32. C. Lyngå, F. Ossler, T. Metz, J. Larsson, Appl. Phys. B **72**, 913 (2001)
33. T.N. Chang, T.K. Fang, Phys. Rev. A **52**, 2052 (1995)
34. Z. Felfli, S. Manson, private communication
35. S. Zamith, V. Blanchet, B. Girard J. Norin, J. Mauritsson, A. L'Huillier, J. Andersson, S.L. Sorensen, I. Hjelte, O. Björneholm, D. Gauyacq, J. Chem. Phys. (in press, 2003)
36. R. López-Martens, J. Mauritsson, A. Johansson, J. Norin, A. L'Huillier, Eur. Phys. J. D **26**, 105 (2003)
37. R. Zerne, C. Altucci, M. Bellini, M.B. Gaarde, T.W. Hänsch, A. L'Huillier, C. Lyngå, C.-G. Wahlström, Phys. Rev. Lett. **79**, 1006 (1997)
38. M. Bellini, C. Lyngå, A. Tozzi, M.B. Gaarde, T.W. Hänsch, A. L'Huillier, C.-G. Wahlström, Phys. Rev. Lett. **81**, 297 (1998)
39. R.A. Bartels, A. Paul, H. Green, H.C. Kapteyn, M.M. Murnane, S. Backus, I.P. Christov, Yanwei Liu, D. Attwood, C. Jacobsen, Science **297**, 377 (2002)
40. D. Xenakis, O. Faucher, D. Charalambidis, C. Fotakis, J. Phys. B **29**, L457 (1996)
41. T. Sekikawa, T. Katsura, S. Miura, S. Watanabe, Phys. Rev. Lett. **88**, 193902 (2002)
42. N.A. Papadogiannis, L.A.A. Nikolopoulos, D. Charalambidis, G.D. Tsakiris, P. Tzallas, K. Witte, Phys. Rev. Lett. (in press, 2003)
43. R. Kienberger, M. Hentschel, M. Uiberacker, Ch. Spielmann, M. Kitzler, A. Scrinzi, M. Wieland, Th. Westerwalbesloh, U. Kleineberg, U. Heinzmann, M. Drescher, F. Krausz, Sciencexpress, `10.1126/science.1073866` (2002)
44. M. Drescher, M. Hentschel, R. Kienberger, M. Uiberacker, V. Yakolev, A. Scrinzi, Th. Westerwalbesloh, U. Kleineberg, U. Heinzmann, F. Krausz, Nature **419**, 803 (2002)